AJNR

Correlation of single photon emission CT with MR image data using fiduciary markers.

B J Erickson and C R Jack, Jr

AJNR Am J Neuroradiol 1993, 14 (3) 713-720
http://www.ajnr.org/content/14/3/713

Correlation of Single Photon Emission CT with MR Image Data Using Fiduciary Markers

Bradley J. Erickson[1] and Clifford R. Jack, Jr.[1]

PURPOSE: To describe our approach to mapping the functional information provided by single photon emission computed tomography (SPECT) onto the anatomic template provided by MR, and to determine both the number of markers required to achieve accuracy and the impact of voxel shape on accuracy. **METHODS:** Point-to-point iterative minimization using externally fixed fiducial markers was involved and computer simulations were performed. Two types of validation studies were performed using a phantom of known dimensions. First, the spatial distortion that may be present in MR was investigated for spin-echo and gradient-recalled echo images. Next, the accuracy with which the SPECT image could be transformed to match the MR template was analyzed. The method is also demonstrated in four cases of patients with epilepsy. **RESULTS:** Computer simulations indicated that for voxel dimensions we expected to use, eight fiduciary markers would consistently produce acceptable accuracy. Simulations also showed that more isotropic voxels would be more accurate if voxel volume is held constant. The spatial accuracy of both spin-echo and gradient-recalled echo images of a phantom was accurate to within 3 mm. When the SPECT image of the same phantom was correlated with the MR image using this technique, internal marker errors were never greater than 3 mm, and the mean error was 2.2 mm. **CONCLUSIONS:** Images from different modalities can be accurately correlated using multiple fiduciary markers. SPECT and MR images of the given dimensions can be correlated to within 3 mm. The technique aids in clarification of the nature of SPECT perfusion abnormalities and in their anatomic localization.

Index terms: Single photon emission computed tomography (SPECT); Images, processing; Magnetic resonance, image display

AJNR 14:713–720, May/Jun 1993

Multiple imaging modalities exist that use different physical phenomena to provide diagnostic information. Computed tomography (CT) and magnetic resonance (MR) imaging provide detailed anatomic information as well as information about the state of tissue hydration, which can often indicate the presence of pathology and possibly the nature of the disease. The addition of contrast agents often improves this delineation. Because of their poor spatial resolution, other modalities such as single photon emission computed tomography (SPECT), positron emission tomography (PET), and biomagnetism emphasize functional information more than anatomic detail. As a result, regional abnormalities that often cannot be localized precisely with respect to individual patient cortical topography would benefit from integration with anatomical examinations. In this paper, we will investigate a method to map the functional information provided by SPECT onto the anatomic template provided by MR. The spatial registration or correlation of SPECT image data with MR was performed and tested using software written by one of us (B.J.E.). The physical accuracy of the method will be demonstrated and example cases shown.

Received February 19, 1992; revision requested May 28; revision received and accepted July 10.

Dr Jack is supported in part by NIH Grant R55NS28374-OA1.

[1] Department of Radiology, Mayo Clinic, 200 First Street SW, Rochester, MN 55905. Address reprint requests to C. R. Jack, MD.

AJNR 14:713–720, May/June 1993 0195-6108/93/1403–0713

Materials and Methods

The Correlation Algorithm

The image correlation process consists of three steps. The first step is to identify the position-of-reference fiduciary markers (small, externally fixed capsules identifiable by both MR and SPECT) in each data set. To accomplish this task quickly and easily, six images are presented to the user—a transaxial, a coronal, and a sagittal image from

each data set. Above each image is a slider bar that identifies the current section number and may be used to select the current image. Alternatively, the user may select a point on one image using a computer pointing device (in this case a mouse); the other two images are then updated so that they intersect the selected position. Lines indicating the planes of intersection are drawn on the images. The corresponding marker in the other volume is then identified. When a marker is identified in each data set, the user clicks on the "accept" button. This process is repeated for each marker. Typically, a few minutes are required to locate the fiduciaries accurately.

The second step is to use these corresponding reference locations to compute the transformation that will match the coordinate system of one data set with the other. There are nine variables that specify the transformation: X, Y, and Z translation; X, Y, and Z rotation; and X, Y, and Z scale factors (equation A). (Note that the center of rotation will be fixed at the origin of the volume.) The algorithm uses known voxel dimensions for scale factors; the positions of the markers are used to calculate the other transformation values. An error function calculates the sum of the distances between the positions of points in one set and the transformed positions of the others. The error function (equation B) is minimized using a modified Brent-Powell (1, 2) method. To assure that the global minimum is reached, several iterations with different initial possible (seed) values are automatically performed. In this way, a local minimum found by an unlucky choice of seed values does not lead to a suboptimal solution.

$$P' = R * ((P * S) - C) + T \quad (A)$$

where

P is the input point vector (X, Y, Z)
P′ is the transformed point vector
R is the 3×3 transformation matrix
S is the scale matrix
C is the translation matrix for center of rotation, and
T is the translation matrix

$$Err = \sum_{i=1}^{N} [P1(i) - P2'(i)]^2 \quad (B)$$

where

P1 (i) is the position of the *i*th marker on MR
P2′ (i) is the transformed position of the *i*th marker on SPECT, and
N is the number of markers

The final step is to use this transformation matrix to reformat geometrically one data set to match the other. In this case, the SPECT data is transformed to match the MR anatomic template. Trilinear interpolation is used to minimize interpolation error.

Simulation Studies

The simulation studies were performed not with an actual phantom, but with an idealized spherical body. To determine the minimum number of markers required to provide acceptably accurate correlated data sets, simulations were performed using the above algorithm on a synthetic data set consisting of 14 arbitrarily chosen locations distributed about the periphery of a spherical volume 18 cm in diameter. (This number was arbitrarily chosen based on the maximum reasonable number of markers the authors felt could be attached to a subject's scalp, with 6 on the midline and 4 on each hemisphere.) These synthetic reference marker positions were rotated and transformed a known amount to create a second set (which mimics the SPECT study). Both sets were then converted to voxel positions based on specified voxel dimensions. Simulations were run using from three to 14 points as reference fiducials, with the error calculated as the difference in location of the markers in the data sets for all 14 points. Repeated simulations (10) were run for each number of points; the points used were randomly selected from the 14 and, therefore, were not necessarily optimally distributed.

Phantom Validation and Clinical Studies

The MR data sets were acquired at 1.5 T on a GE Signa (GE Medical Systems, Milwaukee, WI) system. The lack of significant chemical shift of vaseline at 1.5 T using the default clinical bandwidth of ±16 kHz was confirmed preliminarily. In phantom studies, axial and sagittal gradient-recalled echo (GRE) volumetric (3-D Fourier transform) acquisitions (voxel size was 0.938 mm × 0.938 mm × 1.5 mm) as well as contiguous section sagittal spin-echo (SE) sequences (voxel size was 0.938 mm × 0.938 mm × 3 mm) were used. In clinical cases, only the axial GRE acquisitions were performed. The SPECT data sets were acquired with a three-headed Trionix crystal system (Trionix Research Laboratory, Twinsburg, OH) and reconstructed using the standard reconstruction parameters with cubic voxels measuring 3.56 mm on each side. Data was transferred to a dedicated workstation (RS/6000, IBM Corporation, White Plains, NY) where image correlation was performed.

Each marker consisted of a strand of tissue paper that was soaked with Tc-99m and placed in a 3- to 4-mm section of plastic intravenous tubing. This was placed in a #5 gelatin capsule (6 mm × 4 mm) containing vaseline, which provides signal on T1-weighted MR images. These fiducial capsules, visible on both MR and SPECT, were attached to the phantom (or in clinical cases, to the patient's scalp) for the duration of both imaging studies. The phantom used for verification of accuracy was designed for validation testing in stereotactic neurosurgery. It consisted of a Plexiglas base from which six rods of varying length projected vertically, and a surrounding Plexiglas cylinder bolted to the base. The radius of the cylinder was 7 cm and the height was 18 cm. The fiducial capsules were fixed at the tip of the six internal rods (which ranged in height from 3 cm to 14 cm) within the phantom as well as at eight positions on the outside surface of the cylinder. This phantom mimics the clinical situation: the eight external points represent stereotactic reference points (ie, the fiducials fixed to the scalp (or a headframe) which were

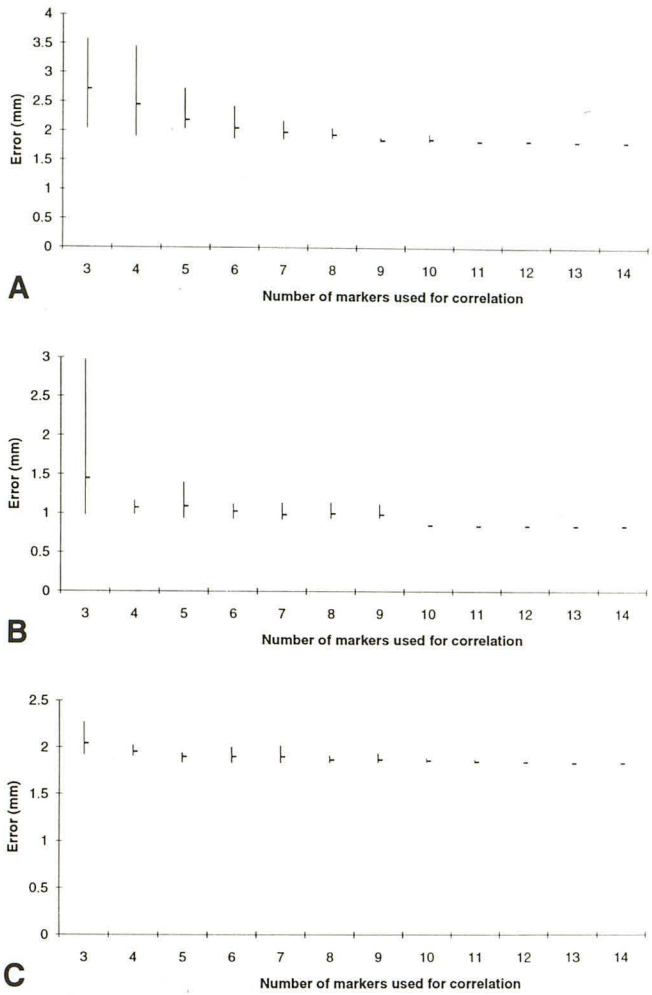

Fig. 1. Simulation study; number of markers versus error (mm).

A, MR voxel size: .938 × .938 × 1.5 and SPECT voxel size: 3.56 × 3.56 × 3.56; *B*, MR = .938 × .938 × 1.5 and SPECT = 2.0 × 2.0 × 2.0; *C*, MR = .938 × .938 × 1.0 and SPECT = 3.56 × 3.56 × 3.56.

used for correlation); the six internal points of the phantom represent target points (ie, discrete sites of patient anatomy to be correlated which thus were not used in computing the correlated images).

Transformation of images was based on location of the reference points; the accuracy of the transformation was calculated using the location of the target points in the transformed images. The precise X, Y, and Z coordinate position of each internal and external marker on the phantom had been measured to an accuracy of 0.1 mm. These were compared with the X, Y, and Z coordinates of both internal and external points that were measured from the images acquired for these experiments. When identifying the position of the fiduciaries on MR scans, the signal void created by the Tc-99m-labeled intravenous tubing could be identified within the vaseline-filled capsules and this was used to select the position of the fiducial marker; the point of greatest intensity was selected on SPECT scans. To tax the correlation program, the phantom was placed in the SPECT scanner rotated approximately 90° relative to its position when imaged by MR.

Two types of validation experiments were performed using the phantom. First, for each of the three MR acquisitions (axial and sagittal GRE and sagittal SE) the positions of the eight external reference markers on the phantom were used to transform the image to the coordinate system used for physically measuring the phantom. This step was necessary because the phantom was not rigidly fixed relative to the scanner. The second part of the validation study tested the accuracy with which the location of the six internal target markers on the SPECT image of the phantom could be transformed using the eight external markers as fiducial reference points. The distance between the positions of the six internal target markers on the MR and the transformed SPECT was computed.

Clinical cases were accrued by identifying patients undergoing evaluation of epilepsy. In these cases, eight reference markers were fixed to the patient's scalp prior to SPECT imaging and removed upon completion of the MR examination. Ictal SPECT studies in both patients were obtained by injecting the isotope (Tc-99m HMPAO) during the somatic ictal behavior; interictal SPECT studies were obtained by injecting the same agent when no seizure activity was occurring.

Results

Simulation Studies

The number of markers used for correlation versus average error for various voxel sizes is shown in Figure 1. Figure 1A depicts this relationship using both the MR and SPECT voxel dimensions that we use for clinical imaging. Previous investigators (3) have postulated that the error is on the order of the lower resolution image, but we have found the relationship to be more complex. Figures 1B and 1C demonstrate that decreasing either the SPECT voxel size *or* the MR voxel size will decrease the average error. The graphs also indicate that with smaller voxels, fewer points would be required to achieve the lower error reliably.

To assess the effect of voxel shape on accuracy, simulations were performed in which the volume of the voxel was held constant (16.25 mm^3 for both the MR and SPECT voxels), but the geometry was altered. A graph of errors for different voxel geometries is given in Figure 2. It is apparent that isotropic voxels produce more precise correlations when voxel volume is held constant.

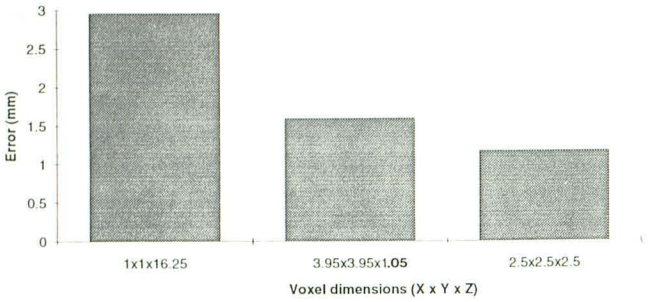

Fig. 2. Simulation study; shape of voxel versus error. Both MR and SPECT voxel volume is held constant (16.25 mm^3) as shape was varied from long and thin to cubic. Dimensions shown are X × Y × Z.

Phantom Studies

Table 1 shows the residuals for the eight external reference markers for each of the three MR studies. The positions of the six internal target markers in the three studies was determined, and the distance from the known measured positions was computed. This error did not exceed 3 mm for the GRE sequence, and averaged less than 3 mm for the SE sequence. Based on this data, we feel safe in concluding that the MR template obtained can accurately represent object geometry, particularly with the 3-D GRE sequence.

The second part of the phantom study addressed the accuracy with which the SPECT images could be transformed onto the MR anatomic template. The eight external reference points (mimicking markers glued to the patient's scalp) were used to transform the SPECT image of the phantom to match the axial GRE image of the phantom. The six internal target points then mimic intracranial anatomic structures and indicate the measured error. Table 2 gives the residuals (ie, the distance between the external reference markers used for computing the transformation) as well as the actual errors (distance in millimeters) for each internal target marker. The average error for the six internal points in the SPECT data was 2.245 mm; no error was greater than 3 mm.

Clinical Studies

Correlative imaging studies of four epilepsy patients are illustrated. In the first two, the SPECT studies were done interictally; in the second two, ictal SPECT studies were obtained. The SPECT studies were performed first and followed immediately by the MR. In the two interictal cases, the correlated images served to clarify the nature of perfusion abnormalities on the SPECT studies. In

TABLE 1: Spatial accuracy of MR

Point	Axial 3-D	Sagittal 3-D	Sagittal SE
Reference			
A	0.659	2.102	2.451
B	0.517	0.207	2.160
C	1.698	2.152	1.197
D	1.083	2.238	2.245
E	0.635	0.111	0.867
F	1.686	1.498	1.458
G	0.770	1.687	2.738
H	1.923	1.728	1.934
Average	1.121	1.465	1.881
Target			
1	2.438	1.786	2.516
2	2.151	1.956	2.903
3	1.632	2.462	2.464
4	2.243	2.663	2.529
5	2.789	2.425	3.251
6	2.367	2.963	2.686
Average	2.270	2.376	2.686

Note.—Reference points A–H were on the surface of the phantom and were used for performing the correlation. The number shown is the error at each point as given in equation B, and represents the maximum accuracy expected. Target points 1–6 were within the cylinder; the value shown is the distance from the known position of the point in the phantom to the imaged position.

TABLE 2: Accuracy of correlation of SPECT with MR

Reference Point	Residual (mm)
A	1.256
B	2.759
C	2.850
D	2.756
E	2.767
F	2.857
G	0.000
H	2.059
Average residual: 1.913 mm	
Target Point	**Error (mm)**
1	2.515
2	2.189
3	2.399
4	1.724
5	1.651
6	2.989
Average error: 2.245 mm	

Note.—Residuals and errors of correlated SPECT data set versus axial 3-D MR data set in millimeters. Points A–H were external reference points used to correlate the SPECT to the MR, and are calculated according to equation B. Points 1–6 were internal target points—the error is the distance between the known position and that calculated from the transformed SPECT image.

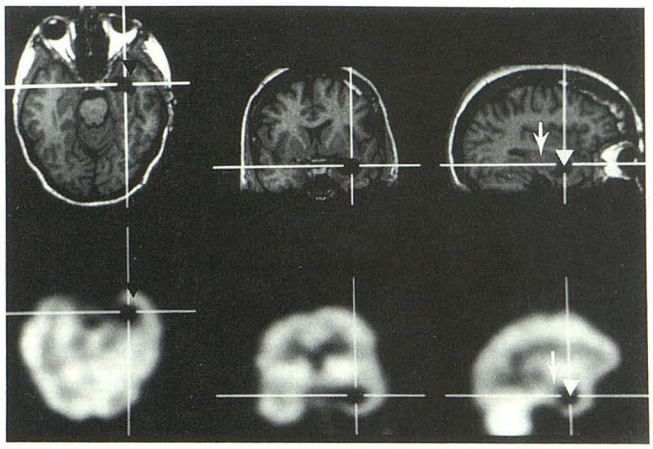

Fig. 3. An interictal scan in which a temporal lobe tumor causes temporal lobe seizure activity. The precise nature of the photopenic area on the SPECT study is ambiguous, but becomes clear after correlation. Tumor (*arrow*), trapped temporal horn (*white arrowhead*), uninvolved temporal cortex (*black arrowhead*).

both cases, the SPECT studies might have been interpreted incorrectly without the insight provided by the correlated images. The patient in Figure 3 had intractable epilepsy caused by a known left temporal lobe glioma that had been biopsied. The photopenic area in the left temporal tip was originally (before correlation) interpreted as a biopsy defect. After correlation, it became apparent that it was the temporal horn, which had been trapped by the growing medial temporal lobe glioma. The correlated images demonstrate precisely the level of isotope activity associated with the three different tissue types in the medial temporal lobe: uninvolved cortex was highest; tumor was intermediate; cerebrospinal fluid in temporal horn was lowest.

In the second case, a left medial frontal photopenic area was originally interpreted to represent the substrate of this patient's left frontotemporal epileptogenic activity, which had been identified on scalp electroencephalogram (EEG). Following correlation, however, this area was shown to represent merely volume averaging of a prominent sulcus. A second photopenic area in the inferior anterior frontotemporal area was originally thought to represent volume averaging of the horizontal portion of the sylvian fissure. After correlation, however, this area is shown to be in the anterior portion of the superior temporal gyrus and is a more likely candidate for the epileptogenic zone (Fig. 4).

The two ictal scans shown here demonstrate the marked and localized increased cerebral perfusion in the region of the seizure focus known to occur during and immediately after ictal activity. The first case (Fig. 5) is a previously normal 9-year-old girl who developed intractable partial motor seizures (focal motor status) involving the left arm and leg following a viral illness. Although not biopsy proved, the clinical, EEG, and MR evidence strongly suggested Rasmussen encephalitis (4). The right frontal cortex is atrophic (particularly inferiorly) with the exception of a small edematous gyrus in the region of the pre-

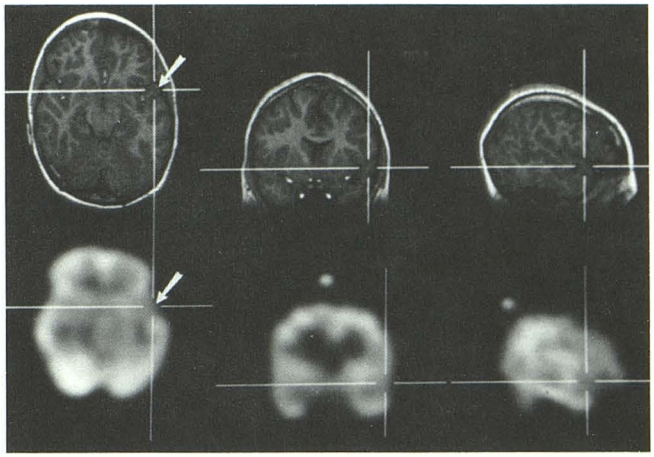

Fig. 4. Interictal scan of a patient with a left frontotemporal lobe scalp EEG focus. *Arrows* demonstrate an area of hypoperfusion on the SPECT scan which was originally interpreted as volume averaging of the horizontal portion of the sylvian fissure. After correlation, however, this area is localized to the anterior part of the superior temporal gyrus.

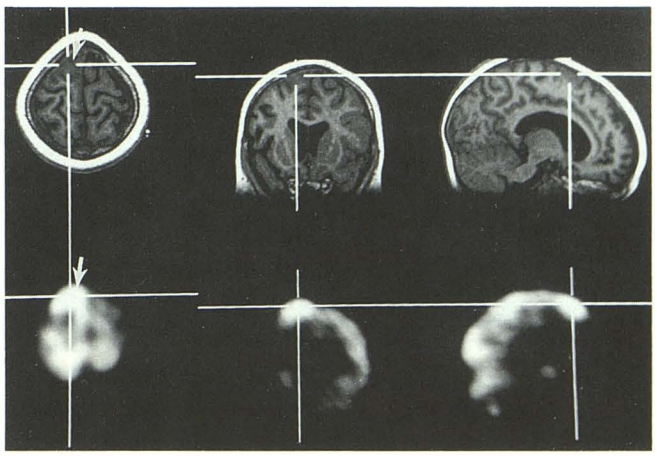

Fig. 5. An ictal scan in a patient with presumed Rasmussen encephalitis. The MR demonstrates a prominent gyrus (*upper arrow*) which corresponds with the area of increased perfusion on SPECT (*lower arrow*). From the correlated images, we postulate that the patient's condition at the time of imaging studies (focal motor status epilepticus) was a result of ongoing cortical inflammation involving the premotor cortex and adjacent motor strip. Note the atrophy of the frontal lobe inferior to this area on the coronal MR and the corresponding hypoperfusion on SPECT.

motor cortex. On ictal SPECT, the atrophic areas are hypoperfused and the edematous area is hyperperfused. This latter area was felt to represent an area of active inflammation and perfectly matched the somatic expression of the patient's seizures.

Figure 6A is an ictal scan of a 50-year-old man who could voluntarily induce focal motor seizures of the left leg. The ictal SPECT scan demonstrates increased perfusion associated with seizure activity. Because surgical resection of the epileptogenic focus was a consideration, it was crucial to identify its exact location. Figure 6B shows a volume rendering of the correlated SPECT combined with the MR. The seizure focus is seen to lie on the precentral gyrus.

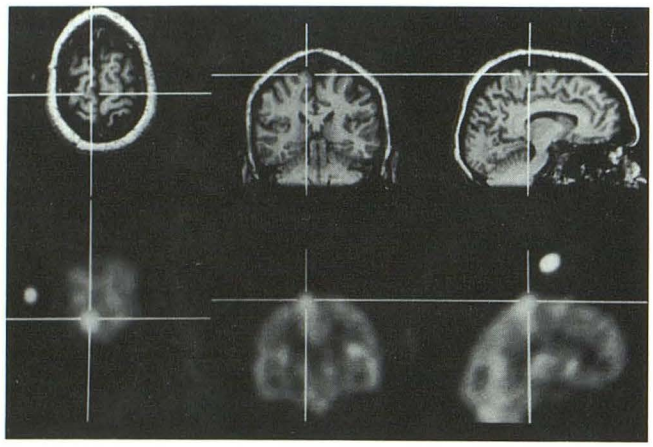

A

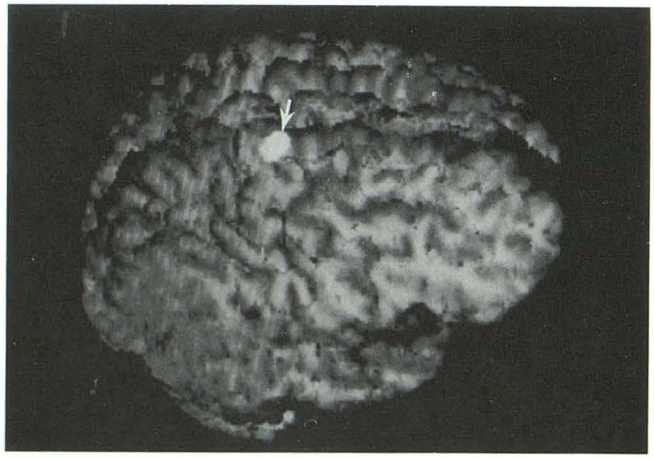

B

Fig. 6. *A*, Ictal scan in a patient with recurrent seizures. Note no structural abnormality is present on MR. There is focal increased perfusion on the SPECT scan when the imaging agent was injected during a voluntarily induced seizure. One of the fiducial reference markers can be seen on both the axial and sagittal MR and SPECT images.

B, Same data set as *A* but using volume-rendering to show 3-D relationship between seizure focus (*arrow*) and cortical topography. The site of the hot spot (the leg portion of the homunculus on the precentral gyrus) perfectly matches the seizure type–focal motor leg. Visualization of this relationship between functional anatomic location and local perfusion abnormality is only possible with integrated images.

Discussion

Despite a growing interest in image correlation and published reports of clinical application, there is little quantitative experimental documentation in the imaging literature addressing the accuracy with which image correlation can be performed. This paper attempts to address that void. Methods for performing point-to-point image correlation and surface matching have been described for correlation of anatomic imaging studies (CT and MR) and PET. The point-to-point method of Arun et al (5) uses four reference fiducial points to compute the rotation and translation factors. Simulations described here suggest that at least eight reference points are necessary with the voxel dimensions used clinically. Point-to-point matching has also been done using traditional neurosurgical stereotactic methods (6) which involve surgically mounting a head frame. Conversely, the technique we describe is noninvasive and, therefore, is widely applicable for diagnostic imaging.

A second approach involves retrospectively matching the skin surface defined by two different imaging studies. This approach has some definite advantages (7) over point-to-point methods, but it also has some weaknesses. No documentation of the accuracy of localization of the "skin" localized by MR versus the "skin" localized by SPECT, PET, or CT has been shown. Furthermore, automated surface tracking is probably impractical for SPECT because of the poor visualization of skin. In a recent report on SPECT-MR surface fitting, it was necessary to trace the brain surface manually on successive 2-D sections, and the apparent accuracy was evaluated in a qualitative fashion (8). A third technique (9) involves the determination of the interhemispheric plane and subsequent interactive, user-determined matching of successive sagittal sections. Error quantification (which averaged 3.8 mm) was based on the standard deviation of the transformation parameters for adjacent sections. Formal studies validating the accuracy of fit by using phantoms of known dimensions have not been published to our knowledge.

The technique we describe is generally applicable, does not rely on the assumption that all modalities image the skin in the same manner,

and does not require a subjective task like tracing or matching a surface. One weakness of this approach is that the markers must be placed prior to imaging: the correlative imaging studies must therefore be planned prospectively. A corollary problem is that it is more difficult to compare studies in time. However, standardization of landmarks may guide the positions of reference fiduciaries, and relatively permanent marks may be made on the skin (as in radiation treatment) to identify marker positions in follow-up studies.

The simulations demonstrate the intuitive concept that improving the resolution of either data set results in a better fit. In the process of conducting this study, we considered the more challenging question of the optimal geometry of voxels, because it can be manipulated by modalities like MR. In the case of MR, it is possible to obtain anisotropic voxels; in fact, for SE techniques, it is nearly obligatory. We have demonstrated that more isotropic voxels provide increased accuracy when the volume of the voxel is held constant.

The possibility that spatial distortion may be present in MR images has not been addressed in previous reports of image correlation; rather, the absolute accuracy of MR has been taken as a given. A recent investigation (W. Pavlicek, personal communication, 1991) indicates that even with state-of-the-art equipment, significant geometric distortion might be present at the periphery of the field of view with GRE acquisitions, and with narrow bandwidth SE acquisitions—hence the need to address the issue of how accurately the MR anatomic template reproduces object geometry.

We evaluated MR accuracy in these experiments for SE and GRE acquisition sequences. We also evaluated the possible effect that the plane of acquisition might have on the spatial accuracy of MR, since nonuniform performance of the different gradient coils has been a problem in the past. While SE sequences are less subject to spatial distortion that is caused by static magnetic field inhomogeneity, they have relatively poorer resolution in the section-select direction than volume acquisitions. This poorer resolution results in the greater error for SE seen in Table 1. The spatial accuracy of 3-D GRE sequences has not, to our knowledge, been documented with respect to a phantom of known physical dimensions. Susceptibility artifacts were of particular concern because of the location of the reference fiducials on the surface (periphery) of the object of interest (spatial warping would be most pronounced at the periphery of the field of view). However, with the (default) bandwidth used, spatial registration errors are not significant regardless of the technique (SE or GRE) or plane of image acquisition. No significant difference in error was apparent between the axial and sagittal sequences.

We are not aware that anyone has fully addressed the question of determining the boundaries of abnormal perfusion on SPECT scans. The method used here (Fig. 6B) finds the boundary of abnormal perfusion by determining the maximum gradient within a user-defined region of interest. This method was chosen because it was objective and seems reasonable. However, more work is needed in this area to document that the borders determined in this fashion correlate with borders of pathologically involved tissue.

Finally, this is the first report to our knowledge describing the correlation and 3-D display of *ictal* SPECT and MR studies. The limited in vitro half-life of Tc-99m HMPAO restricts the clinical applicability of ictal SPECT at this time in North America. However, anticipated future availability of longer lived compounds should enable routine ictal SPECT imaging. We feel that correlated ictal SPECT-MR studies will have a major impact on the management of patients with medically intractable epilepsy.

Conclusions

A novel method for correlating MR and SPECT images has been described and the accuracy of this method has been shown. The investigation included the effect such variables as voxel size and shape have on accuracy. Clinical examples in which accurate correlation of SPECT images with MR proved useful were presented. The ability to view functional information such as that provided by SPECT with anatomic information provided by 3-D MR significantly improves the diagnostic value of either alone. However, it appears reasonable that an accurate method of correlation, such as that described here, is required.

Acknowledgments

We thank Steve Goerss for providing the phantom, and Frank W. Sharbrough, MD, and Robert V. Groover, MD, for recruiting patients for this study.

References

1. Powell MJD. An efficient method for finding the minimum of a function without calculating derivatives. *Comput J* 1964;7:155
2. Brent RP. *Algorithms for minimization without derivatives.* Englewood Cliffs, NJ: Prentice-Hall, 1973:67–83
3. Levin DN, Pelizzari CA, Chen GTY, et al. Retrospective geometric correlation of MR, CT and PET images. *Radiology* 1988;169:817–823
4. Aguilar MJ, Rasmussen T. Role of encephalitis in pathogenesis of epilepsy. *Arch Neurol* 1960;2:663–676
5. Arun KS, Huang TS, Blostein SD. Least squares fitting of two 3D point sets. IEEE t-PAMI 1987;9:698–700
6. Kearfott KJ, Rottenberg DA, Knowles RJR. A new headholder for PET, CT, and NMR imaging. *J Comput Assist Tomogr* 1984;8:1217–1220
7. Chen GTY, Pelizzari CA. Image correlation techniques in radiation therapy treatment planning. *Comput Med Imaging Graphics* 1989;13:235–240
8. Holman BL, Zimmerman RE, Johnson KA, et al. Computer-assisted superimposition of magnetic resonance and high-resolution technetium-99m-HMPAO and Thallium-201 SPECT images of the brain. *J Nuc Med* 1991;32:1478–1484
9. Kapouleas I, Alavi A, Alves WM, Gur RE, Weiss DW. Registration of three-dimensional MR and PET images of the human brain without markers. *Radiology* 1991;181:731–739